Spontaneous Crystallization in Systems of Binary Hard Sphere Colloids

Praveen K. Bommineni, Marco Klement, and Michael Engel*
Institute for Multiscale Simulation, IZNF, Friedrich-Alexander University Erlangen-Nürnberg, Cauerstrasse 3, 91058 Erlangen, Germany

(Received 12 December 2019; accepted 8 May 2020; published 28 May 2020)

Computer simulations of the fluid-to-solid phase transition in the hard sphere system were instrumental for our understanding of crystallization processes. But while colloid experiments and theory have been predicting the stability of several binary hard sphere crystals for many years, simulations were not successful to confirm this phenomenon. Here, we report the growth of binary hard sphere crystals isostructural to Laves phases, AlB_2, and $NaZn_{13}$ in simulation directly from the fluid. We analyze particle kinetics during Laves phase growth using event-driven molecular dynamics simulations with and without swap moves that speed up diffusion. The crystallization process transitions from nucleation and growth to spinodal decomposition already deep within the fluid-solid coexistence regime. Finally, we present packing fraction–size ratio state diagrams in the vicinity of the stability regions of three binary crystals.

DOI: 10.1103/PhysRevLett.124.218003

Introduction.—Hard spheres are arguably one of the simplest particle model. Their crystallization is a classic example of a phase transition discovered by computer simulation [1–3]. A prediction of the model is the spontaneous ordering of concentrated suspensions of nearly hard colloidal spheres [4]. Generalizations are mixtures of spheres with different sizes such that small spheres fit between large spheres to stabilize binary crystals. Early experimental realizations are binary crystals isostructural to AlB_2 and $NaZn_{13}$ found in natural opal gems [5–7]. More recent experiments [8–12] and theory [13–20] predicted additional ones. By now, four binary crystals have been proposed in the hard sphere phase diagram near the solidus line: NaCl ($0.30 \leq \alpha \leq 0.41$), AlB_2 ($0.45 \leq \alpha \leq 0.62$), $NaZn_{13}$ ($0.54 \leq \alpha \leq 0.61$), and Laves $MgCu_2$ and $MgZn_2$ ($0.76 \leq \alpha \leq 0.84$). This list identifies binary crystals by their atomic prototype and contains the reported ranges for size ratio $\alpha = \sigma_S/\sigma_L$, where σ_S and σ_L are the diameters of small and large spheres, respectively. Additional binary crystals, such as CsCl [11], are believed to be metastable or appear only at high packing fraction ϕ as densest packings [21–23].

Equal-sized hard spheres crystallize rapidly into the face-centered-cubic (fcc) crystal or stacking variants thereof in simulation, and they have been an ideal testing ground for studying fundamental aspects of crystal nucleation and growth [24–26]. It was thus expected that simulations of binary hard sphere fluids produce binary crystals in a similar manner. This has not been the case. To date, the only binary hard sphere crystal growth reported in simulation is NaCl [18]. That report is more than 20 years old, and the crystals grown are highly defective with many vacancies of the small spheres [27,28]. AlB_2 so far required a seeding procedure to grow [29]. Laves phases and $NaZn_{13}$ formed from size-disperse sphere fluids only with the assistance of Monte Carlo swap or resize moves [30,31] and nearly hard spheres where particle softness enhances crystallization [32]. The absence of binary hard sphere crystallization in simulation has been puzzling. Here, we report the spontaneous formation of AlB_2, $NaZn_{13}$, and Laves phases in simulation directly from the fluid. Our results demonstrate that binary hard sphere crystals grow robustly and reproducibly in standard event-driven molecular dynamics (EDMD) given only sufficient simulation time and large enough system size. Surprisingly, Laves phases crystallize via nucleation and growth as well as via spinodal decomposition. We find that the bottleneck for binary crystal growth is diffusion in the dense fluid.

Growth of Laves phase.—Laves phases are of relevance for materials scientists because they are the most common binary intermetallic compounds [33] and have interesting photonic properties when self-assembled from colloids [34]. For this reason, we focus on their growth first. We speed up crystallization in an initial test by combining EDMD simulations with swap moves [30,31,35–40]. Particle pairs are attempted to be swapped as a Monte Carlo move at every collision [41]. Gibbs free-energy calculations [19] guide us to the parameter set $(\phi, \alpha) = (0.57, 0.80)$, which lies in the fluid-Laves coexistence regime slightly below the solidus line. We initialize a simulation at composition LS_2 in the fluid state and run it at isochoric (constant volume) conditions with periodic boundaries. The ordering progress of our system is monitored by recording reduced pressure $P^* = P/\Pi$ over reduced simulation time $t^* = t/\tau$. Here, $\Pi = k_B T/V_L$ with volume of the large sphere $V_L = \pi\sigma_L^3/6$ is a unit of pressure and $\tau = \sigma_L\sqrt{m/k_B T}$ is a unit of time.

Pressure evolution is shown as a blue curve in Fig. 1(a). After a rapid initial relaxation of the fluid over time $3 \times 10^3\tau$, pressure decreases slowly while the system starts

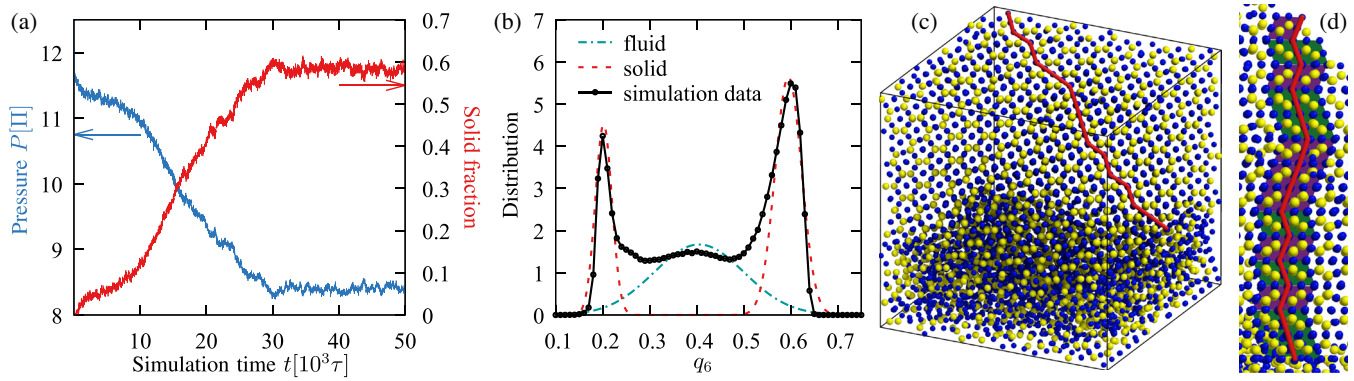

FIG. 1. Crystallization of the Laves phase from a binary hard sphere fluid using a hybrid EDMD simulation with swap moves. The system contains 9999 particles at composition LS_2 and is simulated at $(\phi, \alpha) = (0.57, 0.80)$. (a) Evolution of pressure (blue) and solid fraction (red) with simulation time. (b) Distribution of local bond-orientational order parameters q_6 at fluid-solid coexistence. Solid fraction is computed by fitting the distribution with three Gaussians as indicated by dashed curves. (c) Final snapshot and (d) enlarged view of the simulation showing the coexistence of Laves phase and fluid. Large spheres are represented by yellow color, small spheres by blue color. Particles are drawn at 50% of their size for better visibility. Red line indicates the stacking sequence.

ordering, then gradually faster, until it reaches a constant slope. Crystalline order in the system is well characterized by the q_6 local bond-orientational order parameter [41–43]. The distribution of q_6 values in the system shows pronounced peaks [Fig. 1(b)], which can be assigned to the fluid (broad central peak) and the two particle species in the solid (narrow outer peaks). We fit the peaks to compute solid fraction. Evolution of solid fraction [red curve in Fig. 1(a)] essentially mirrors the evolution of pressure and increases in sync with the pressure drop. The slopes of both curves come to an abrupt halt at $t = 30 \times 10^3\tau$, indicating the end of the crystallization process. After this time, the system reached an equilibrium of about equal amounts of fluid and solid in coexistence.

A snapshot of the equilibrated system viewed along a twofold symmetry axis [Fig. 1(c)] confirms the coexistence. In projection, particles are arranged into columns in the crystal (top part) and are disordered in the fluid (bottom part). The pattern of the crystal in this projection consists of straight rows of small spheres separated by zigzag rows of pairs of large spheres alternating with single small spheres. Such a pattern is characteristic of Laves phases. We extract the stacking sequence of the Laves phase as indicated by the red line in Figs. 1(c) and 1(d). Hexagonal Laves $MgZn_2$ ($C14$) has ABA stacking, which gives a zigzag line. Cubic Laves $MgCu_2$ ($C15$), on the other hand, has ABC stacking, which results in a straight line. We observe both straight and zigzag segments along the red line, demonstrating that our Laves phase is a stacking of $C14$ slabs and $C15$ slabs. In this sense, Laves phase crystallization in our binary system resembles crystallization of identical spheres, which forms stacking variants of fcc.

Laves phase crystallization pathway.—Our simulation in Fig. 1 established Laves phase growth from the binary hard sphere fluid using swap moves rather easily. To show reproducibility and generality, we perform ten swap simulations and ten nonswap simulations at the same parameters and with similar initial conditions. Well-ordered Laves phases form in all 20 simulations. Both simulation methods lead to similar pressure-time pathways (Fig. S1 in the Supplemental Material [41]), even though the speed in which these pathways are traversed is different. As expected, swap simulations are significantly faster in crystallizing the binary fluid. The speed-up is not constant but increases from 20× to 120× [Fig. 2(a)], demonstrating that the efficiency of swap moves improves over time. Indeed, the acceptance probability of swap moves increases over the same time window (Fig. S2 in the Supplemental Material [41]). This indicates an increase in available free volume in the fluid and explains the higher speed-up toward the end of the simulation. Swap moves primarily enhance diffusion. We conclude that particles are integrated faster into the crystal than they diffuse through the fluid. Therefore, diffusion in the fluid is the bottleneck process for Laves phase growth.

We analyze one exemplary nonswap simulation pathway in more detail by tracking crystalline clusters. Figure 3(a) shows the evolution of the number of clusters and the size of the three largest clusters. A particle is identified as solidlike using a q_6 cutoff (Fig. S3 in the Supplemental Material [41]). A solidlike particle belongs to a cluster if it has more than five solidlike particles within distance $1.1\sigma_L$. Already right at the start of the simulation, ten clusters are detected, indicating there is a very small or negligible free-energy barrier for the Laves phase to form. The clusters grow independently, and their number decreases when they merge, which is also directly apparent in simulation snapshots at increasing times [Figs. 3(b)–3(e)]. After this time, the solid consolidates by removing grain boundaries and transforms its polycrystalline state into a Laves phase single crystal. A video of the growth process for the time window $0 \leq t \leq 2 \times 10^6\tau$ is contained as Supplemental Material [41].

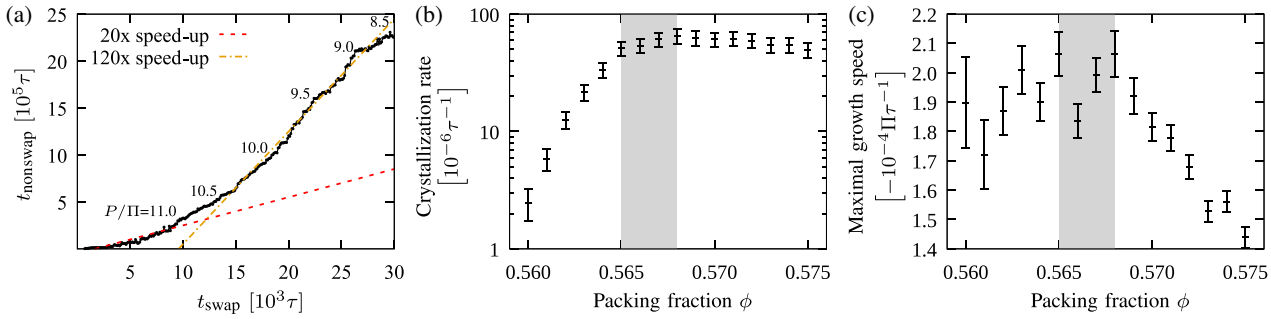

FIG. 2. Laves phase growth kinetics. Simulation parameters and conditions as in Fig. 1. (a) Simulation times necessary to reach certain pressure values in swap and nonswap simulations are compared on the two plot axes. The speed-ups for early and late crystallization are indicated by dashed lines. (b) Crystallization rate gives the inverse mean time to find a growing crystal in a simulation. As density increases, we see a transition from rare nucleation events to nearly constant crystallization rates for spinodal decomposition. Error bars indicate the spread assuming nucleation and growth as the mechanism. (c) Maximal growth speed is defined as the fastest pressure drop and is highest in the transition region (gray area). Weak oversaturation lowers the entropy gain of an ordered structure, and high density slows diffusion. Both factors are balanced at the onset of spinodal decomposition. Data points in (a) and (b), (c) are averaged over ten and 50 runs, respectively. Error bars show the standard error.

Overall, Laves phase growth in this simulation proceeds not as predicted by classical nucleation theory but as expected from spinodal decomposition. This is surprising given that our simulation parameters are chosen below the solidus line in the coexistence regime (Fig. S4 in the Supplemental Material [41]).

Our results so far do not exclude a nucleation and growth regime at lower packing fraction closer to the liquidus line. We analyze the type of crystallization transition by performing 15×50 swap simulations across the packing fraction range $0.56 \leq \phi \leq 0.575$. Indeed, the crystallization rate grows rapidly at $\phi \leq 0.565$ as expected for nucleation and growth and then saturates [Fig. 2(b)]. At the same time, the maximal crystal growth speed decays from a plateau for $\phi \geq 0.568$ as expected for spinodal decomposition [Fig. 2(c)]. Together, our analysis indicates a transition from nucleation-and-growth behavior with stochastic onset of crystallization to spinodal-decomposition behavior where crystallization pathways collapse. This transition is also apparent directly in the evolution of pressure curves (Fig. S5 in the Supplemental Material [41]).

Binary crystal state diagrams.—So far, we investigated binary crystal growth for a specific set of parameters in detail. Now, we vary the packing fraction ϕ and size ratio α more systematically to obtain full state diagrams. We focus on the compositions LS_2 and LS_{13}, for which binary crystals have been predicted. Simulations run for a total time of $2 \times 10^6\tau$. Simulations that crystallize undergo their phase transition completely and fully grow into well-ordered crystals.

We start with composition LS_2. Figure 4(a) shows the state diagram in the vicinity of Laves phases and Fig. 4(b) the state diagram in the vicinity of AlB_2. Both binary crystals form over extended parameter regions. The size ratio range for the Laves phases, $0.76 \leq \alpha \leq 0.86$, and the

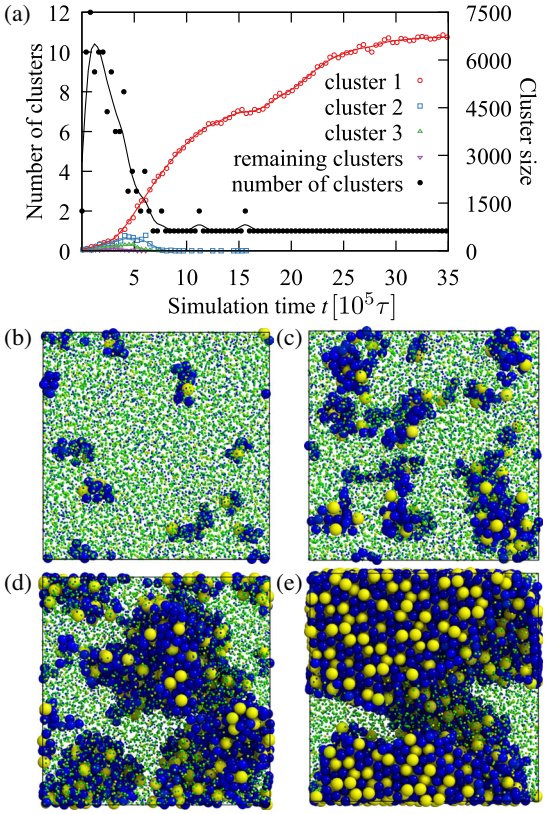

FIG. 3. Exemplary Laves phase growth pathway from a nonswap simulation. Simulation parameters and conditions as in Fig. 1. (a) Evolution of the number of clusters and the sizes of the three largest clusters ("cluster 1" to "cluster 3"). Simulation snapshots at times (b) $t = 2 \times 10^3\tau$, (c) $t = 10^5\tau$, (d) $5 \times 10^5\tau$, and (e) $2 \times 10^6\tau$. Particles are colored according to their local environment. Blue particles have high q_6, yellow particles low q_6. Green particles have intermediate q_6 corresponding to a fluidlike environment. Nonclustered particles are drawn with reduced size for better visibility.

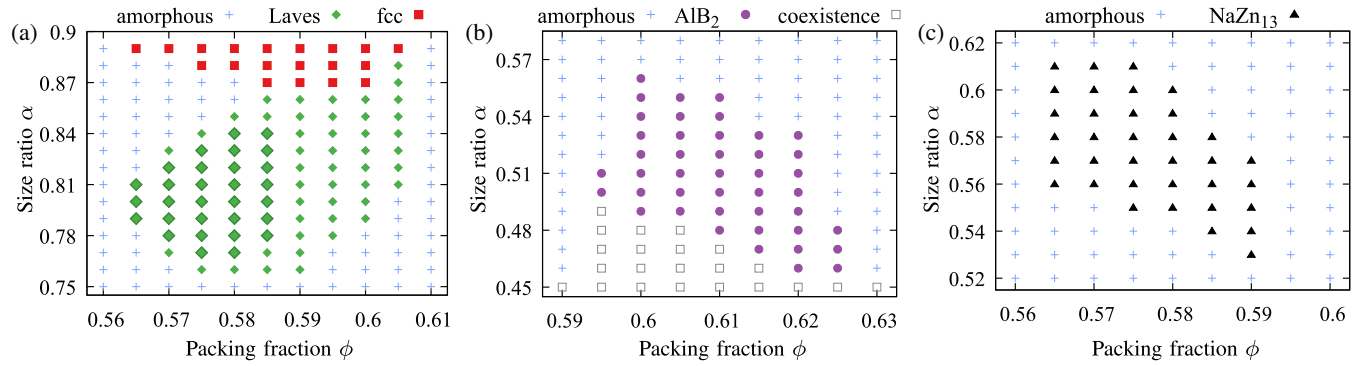

FIG. 4. Packing fraction–size ratio state diagrams in the vicinity of the stability regions of the three binary hard sphere crystals isostructural to (a) Laves phases, (b) AlB_2, and (c) $NaZn_{13}$. Crystal structures are identified using bond-orientational order diagrams and directly in snapshots (see Figs. S6 and S7 in the Supplemental Material [41] and Ref. [44]). Systems contain 1200 particles at composition LS_2 in (a), (b) and 896 particles at composition LS_{13} in (c). Simulations in (a) are run with swaps; large symbols represent Laves phase formation in nonswap simulations. Nonswap simulations crystallize less readily, which is apparent near the boundary of the stability regime and at high packing fraction. Simulations in (b), (c) are run without swaps because the acceptance probability of swap moves is too low for swaps to be useful. At each state point, simulations are repeated twice, and phases reported are observed at least once in simulation.

lower limit of size ratio for AlB_2, $\alpha = 0.46$, agree with predicted values [13,19]. For $0.57 \leq \alpha \leq 0.75$, the system remains amorphous. For $\alpha \leq 0.45$, the binary fluid phase separates into coexisting NaCl and AlB_2 solids. For $\alpha \geq 0.87$, the fluid forms the substitutionally disordered fcc solid.

Results for composition LS_{13} are shown in Fig. 4(c). The binary crystal found at this composition, $NaZn_{13}$, is a complex arrangement of large spheres on a simple cubic lattice and icosahedra made from 13 small spheres at body-centered positions. $NaZn_{13}$ forms in the range $0.54 \leq \alpha \leq 0.61$ as predicted by free-energy calculation [14,15]. The range of packing fractions, for which crystallization is observed, is for all three binary crystals about 3%. Growth of AlB_2 is more difficult and leads to more defects than growth of Laves phases and $NaZn_{13}$, possibly because it occurs at higher packing fractions.

Discussion and conclusions.—Our findings demonstrate that binary crystal growth from the binary hard sphere fluid is robust and reproducible. Why then have similar binary hard sphere crystals not been seen in simulation before? We are not sure. But we can list a few arguments that indicate doing so is not necessarily trivial. In simulations, growth without swap moves requires more than two weeks of continuous simulation with today's fastest processors at the right parameters to obtain well-defined crystals that are easy to identify. Our longest simulations ran for more than four weeks. While this is not a particularly long simulation time, it clearly exceeds typical hard sphere simulation times. EDMD simulations cannot be parallelized efficiently. Furthermore, many simulations in the past used Monte Carlo simulation instead of EDMD, which slows down the growth process further by about one order of magnitude [45].

We map our simulations on two experimental conditions: magnesium atoms and polystyrene colloids. The unit of time for magnesium atoms at a temperature slightly below the solidus line for hexagonal Laves $MgZn_2$, $T = 850$ K, corresponds to $\tau = 0.6$ ps [41]. An atom takes on average about the time τ to move over its diameter. We estimate that Laves phase crystallization requires an experimental time of $10^7\tau = 10$ μs to form nanocrystalline grains. Such times are easily reachable. This explains why Laves phases are ubiquitous in alloys. Colloidal particles, on the other hand, are much larger and slowed down by drag in solution. It is possible to account for most of the effects of hydrodynamic interactions by rescaling the timescale for nucleation and growth by the long-time diffusion coefficient [46]. We use the Stokes-Einstein equation to estimate $\tau = 0.2$ s for colloids with diameter 1 μm suspended in water [41]. Only crystallization of identical hard sphere colloids into fcc has been achieved with such large particles as it is about 10^3 times faster than Laves phase crystallization, even though the softness of charged spheres seems to help obtain a variety of binary structures [47–50]. Crystallization speeds up proportional to σ^{-3} with shrinking colloid diameter σ. Experiments with $\sigma_L = 170$ nm colloids need to rest for months at the optimal condition to form Laves phases [12], which corresponds to an equilibration time of $10^9\tau$ to $10^{10}\tau$ to grow macroscale crystals. Even smaller ≤ 10 nm nanoparticles crystallize rather easily into binary superlattices [51–54].

There have been concerns that swaps alter phase transformation pathways because they preferentially accelerate specific aspects of kinetics. At least for the processes investigated here, crystallization of hard sphere Laves phases, trajectories with and without swap are indistinguishable. If these observations are confirmed in more

systems, then swaps [30,31,35–40] can become a standard tool for simulating mixtures, in particular those with small size difference. Swap methods have the potential to speed up such simulations by orders of magnitude. Finally, our findings add to the growing list of recent observations of crystallization processes in model systems that were once believed to be good glass formers [31,32,37,55,56]. Knowledge of crystal structures competing with the amorphous state, as we report here for the binary hard sphere fluid, is important to ensure that the analysis of local order and particle dynamics [57–59] in such model systems intended for glasses is not affected by hidden crystallization transitions.

In conclusion, this work constitutes the first systematic simulation study of binary crystallization across composition and thermodynamic parameters. Our finding of a transition from nucleation and growth to spinodal decomposition inside the fluid-solid coexistence demonstrates a clear difference of the crystallization behavior of binary hard sphere mixtures as compared to the crystallization behavior of identical hard spheres.

Funding by Deutsche Forschungsgemeinschaft through Project No. EN 905/2-1, support from the Central Institute for Scientific Computing, the Interdisciplinary Center for Functional Particle Systems, and computation resources provided by the Erlangen Regional Computing Center are gratefully acknowledged.

*michael.engel@fau.de

[1] B. J. Alder and T. E. Wainwright, Phase transition for a hard sphere system, J. Chem. Phys. **27**, 1208 (1957).
[2] W. W. Wood and J. D. Jacobson, Preliminary results from a recalculation of the Monte Carlo equation of state of hard spheres, J. Chem. Phys. **27**, 1207 (1957).
[3] B. J. Alder and T. E. Wainwright, Studies in molecular dynamics. II. Behavior of a small number of elastic spheres, J. Chem. Phys. **33**, 1439 (1960).
[4] P. N. Pusey and W. van Megen, Phase behaviour of concentrated suspensions of nearly hard colloidal spheres, Nature (London) **320**, 340 (1986).
[5] J. V. Sanders and M. J. Murray, Ordered arrangements of spheres of two different sizes in opal, Nature (London) **275**, 201 (1978).
[6] J. V. Sanders, Close-packed structures of spheres of two different sizes I. Observations on natural opal, Philos. Mag. A **42**, 705 (1980).
[7] M. J. Murray and J. V. Sanders, Close-packed structures of spheres of two different sizes II. The packing densities of likely arrangements, Philos. Mag. A **42**, 721 (1980).
[8] P. Bartlett, R. H. Ottewill, and P. Pusey, Freezing of binary mixtures of colloidal hard spheres, J. Chem. Phys. **93**, 1299 (1990).
[9] P. Bartlett, R. H. Ottewill, and P. N. Pusey, Superlattice Formation in Binary Mixtures of Hard-Sphere Colloids, Phys. Rev. Lett. **68**, 3801 (1992).
[10] N. Hunt, R. Jardine, and P. Bartlett, Superlattice formation in binary mixtures of hard-sphere colloids, Phys. Rev. E **62**, 900 (2000).
[11] A. B. Schofield, P. N. Pusey, and P. Radcliffe, Stability of the binary colloidal crystals AB2 and AB13, Phys. Rev. E **72**, 031407 (2005).
[12] N. Schaertl, D. Botin, T. Palberg, and E. Bartsch, Formation of Laves phases in buoyancy matched hard sphere suspensions, Soft Matter **14**, 5130 (2018).
[13] M. D. Eldridge, P. A. Madden, and D. Frenkel, A computer simulation investigation into the stability of the AB2 superlattice in a binary hard sphere system, Mol. Phys. **80**, 987 (1993).
[14] M. D. Eldridge, P. A. Madden, and D. Frenkel, Entropy-driven formation of a superlattice in a hard-sphere binary mixture, Nature (London) **365**, 35 (1993).
[15] M. Eldridge, P. Madden, and D. Frenkel, The stability of the AB13 crystal in a binary hard sphere system, Mol. Phys. **79**, 105 (1993).
[16] X. Cottin and P. A. Monson, A cell theory for solid solutions: Application to hard sphere mixtures, J. Chem. Phys. **99**, 8914 (1993).
[17] X. Cottin and P. A. Monson, Substitutionally ordered solid solutions of hard spheres, J. Chem. Phys. **102**, 3354 (1995).
[18] E. Trizac, M. D. Eldridge, and P. A. Madden, Stability of the AB crystal for asymmetric binary hard sphere mixtures, Mol. Phys. **90**, 675 (1997).
[19] A. P. Hynninen, L. Filion, and M. Dijkstra, Stability of LS and LS2 crystal structures in binary mixtures of hard and charged spheres, J. Chem. Phys. **131**, 064902 (2009).
[20] M. Dijkstra, Entropy-Driven Phase Transitions in Colloids: From spheres to anisotropic particles, Adv. Chem. Phys. **156**, 35 (2014).
[21] P. I. O'Toole and T. S. Hudson, New high-density packings of similarly sized binary spheres, J. Phys. Chem. C **115**, 19037 (2011).
[22] L. Filion and M. Dijkstra, Prediction of binary hard-sphere crystal structures, Phys. Rev. E **79**, 046714 (2009).
[23] A. B. Hopkins, F. H. Stillinger, and S. Torquato, Densest binary sphere packings, Phys. Rev. E **85**, 021130 (2012).
[24] S. Auer and D. Frenkel, Prediction of absolute crystal-nucleation rate in hard-sphere colloids, Nature (London) **409**, 1020 (2001).
[25] S. Punnathanam and P. A. Monson, Crystal nucleation in binary hard sphere mixtures: A Monte Carlo simulation study, J. Chem. Phys. **125**, 024508 (2006).
[26] R. Ni, F. Smallenburg, L. Filion, and M. Dijkstra, Crystal nucleation in binary hard-sphere mixtures: The effect of order parameter on the cluster composition, Mol. Phys. **109**, 1213 (2011).
[27] E. C. M. Vermolen, A. Kuijk, L. C. Filion, M. Hermes, J. H. J. Thijssen, M. Dijkstra, and A. Van Blaaderen, Fabrication of large binary colloidal crystals with a NaCl structure, Proc. Natl. Acad. Sci. U.S.A. **106**, 16063 (2009).
[28] L. Filion, M. Hermes, R. Ni, E. C. M. Vermolen, A. Kuijk, C. G. Christova, J. C. P. Stiefelhagen, T. Vissers, A. van Blaaderen, and M. Dijkstra, Self-Assembly of a Colloidal Interstitial Solid with Tunable Sublattice Doping, Phys. Rev. Lett. **107**, 168302 (2011).

[29] P. K. Bommineni and S. N. Punnathanam, Molecular simulation of homogeneous crystal nucleation of AB2 solid phase from a binary hard sphere mixture, J. Chem. Phys. **147**, 064504 (2017).
[30] B. A. Lindquist, R. B. Jadrich, and T. M. Truskett, Communication: From close-packed to topologically close-packed: Formation of Laves phases in moderately polydisperse hard-sphere mixtures, J. Chem. Phys. **148**, 191101 (2018).
[31] P. K. Bommineni, N. R. Varela-Rosales, M. Klement, and M. Engel, Complex Crystals from Size-Disperse Spheres, Phys. Rev. Lett. **122**, 128005 (2019).
[32] T. Dasgupta, G. M. Coli, and M. Dijkstra, Tuning the glass transition: Enhanced crystallization of the laves phases in nearly hard spheres, ACS Nano **14**, 3957 (2020).
[33] W. Steurer and J. Dshemuchadse, *Intermetallics—Structures, Properties, and Statistics* (Oxford University Press, New York, 2016).
[34] A.-P. Hynninen, J. H. J. Thijssen, E. C. M. Vermolen, M. Dijkstra, and A. van Blaaderen, Self-assembly route for photonic crystals with a bandgap in the visible region, Nat. Mater. **6**, 202 (2007).
[35] L. Berthier, D. Coslovich, A. Ninarello, and M. Ozawa, Equilibrium Sampling of Hard Spheres Up to the Jamming Density, and Beyond, Phys. Rev. Lett. **116**, 238002 (2016).
[36] M. Wyart and M. E. Cates, Does a Growing Static Length Scale Control the Glass Transition?, Phys. Rev. Lett. **119**, 195501 (2017).
[37] D. Coslovich, M. Ozawa, and L. Berthier, Local order and crystallization of dense polydisperse hard spheres, J. Phys. Condens. Matter **30**, 144004 (2018).
[38] C. Brito, E. Lerner, and M. Wyart, Theory for Swap Acceleration near the Glass and Jamming Transitions for Continuously Polydisperse Particles, Phys. Rev. X **8**, 031050 (2018).
[39] L. Berthier, E. Flenner, C. J. Fullerton, C. Scalliet, and M. Singh, Efficient swap algorithms for molecular dynamics simulations of equilibrium supercooled liquids, J. Stat. Mech. (2019) 064004.
[40] M. Mihalkovič and M. Widom, Spontaneous formation of thermodynamically stable Al-Cu-Fe icosahedral quasicrystal from realistic atomistic simulations, Phys. Rev. Research **2**, 013196 (2020).
[41] See Supplemental Material at http://link.aps.org/supplemental/10.1103/PhysRevLett.124.218003 for additional text on simulation methods, detection of crystalline clusters, mapping of simulations to experiments, and a video of Laves phase growth.
[42] P. J. Steinhardt, D. R. Nelson, and M. Ronchetti, Bond-orientational order in liquids and glasses, Phys. Rev. B **28**, 784 (1983).
[43] J. A. van Meel, L. Filion, C. Valeriani, and D. Frenkel, A parameter-free, solid-angle based, and nearest-neighbor algorithm, J. Chem. Phys. **136**, 234107 (2012).
[44] M. Engel, P. F. Damasceno, C. L. Phillips, and S. C. Glotzer, Computational self-assembly of a one-component icosahedral quasicrystal, Nat. Mater. **14**, 109 (2015).
[45] M. Klement and M. Engel, Efficient equilibration of hard spheres with Newtonian event chains, J. Chem. Phys. **150**, 174108 (2019).
[46] M. Tateno, T. Yanagishima, J. Russo, and H. Tanaka, Influence of Hydrodynamic Interactions on Colloidal Crystallization, Phys. Rev. Lett. **123**, 258002 (2019).
[47] S. Hachisu and S. Yoshimura, Optical demonstration of crystalline superstructures in binary mixtures of latex globules, Nature (London) **283**, 188 (1980).
[48] P. Bartlett and A. I. Campbell, Three-Dimensional Binary Superlattices of Oppositely Charged Colloids, Phys. Rev. Lett. **95**, 128302 (2005).
[49] M. E. Leunissen, C. G. Christova, A. P. Hynninen, C. P. Royall, A. I. Campbell, A. Imhof, M. Dijkstra, R. van Roij, and A. van Blaaderen, Ionic colloidal crystals of oppositely charged particles, Nature (London) **437**, 235 (2005).
[50] R. A. LaCour, C. S. Adorf, J. Dshemuchadse, and S. C. Glotzer, Influence of softness on the stability of binary colloidal crystals, ACS Nano **13**, 13829 (2019).
[51] E. V. Shevchenko, D. V. Talapin, S. O'Brien, and C. B. Murray, Polymorphism in AB13 nanoparticle superlattices: An example of semiconductor-metal metamaterials, J. Am. Chem. Soc. **127**, 8741 (2005).
[52] E. V. Shevchenko, D. V. Talapin, N. A. Kotov, S. O'Brien, and C. B. Murray, Structural diversity in binary nanoparticle superlattices, Nature (London) **439**, 55 (2006).
[53] W. H. Evers, B. D. Nijs, L. Filion, S. Castillo, M. Dijkstra, and D. Vanmaekelbergh, Entropy-driven formation of binary semiconductor-nanocrystal superlattices, Nano Lett. **10**, 4235 (2010).
[54] I. Coropceanu, M. A. Boles, and D. V. Talapin, Systematic mapping of binary nanocrystal superlattices: The role of topology in phase selection, J. Am. Chem. Soc. **141**, 5728 (2019).
[55] U. R. Pedersen, T. B. Schrøder, and J. C. Dyre, Phase Diagram of Kob-Andersen-Type Binary Lennard-Jones Mixtures, Phys. Rev. Lett. **120**, 165501 (2018).
[56] T. S. Ingebrigtsen, J. C. Dyre, T. B. Schrøder, and C. P. Royall, Crystallization Instability in Glass-Forming Mixtures, Phys. Rev. X **9**, 031016 (2019).
[57] J. F. Robinson, F. Turci, R. Roth, and C. P. Royall, Morphometric Approach to Many-Body Correlations in Hard Spheres, Phys. Rev. Lett. **122**, 068004 (2019).
[58] S. Marín-Aguilar, H. H. Wensink, G. Foffi, and F. Smallenburg, Tetrahedrality Dictates Dynamics in Hard Sphere Mixtures, Phys. Rev. Lett. **124**, 208005 (2020).
[59] M. Campo and T. Speck, Dynamical coexistence in moderately polydisperse hard-sphere glasses, J. Chem. Phys. **152**, 014501 (2020).